Design of a Side-Coupled Linear Accelerator Structure for Linac4

E. Benedico Mora, M. Vretenar

CERN, Geneva, Switzerland

Abstract

In Linac 4, proposed as a future H^- linear accelerator for CERN, a Side-Coupled Linac (SCL) structure will accelerate the beam from 90 MeV to 160 MeV. This note presents the preliminary SCL design, including 2D and 3D RF structure design, layout optimisation, setting up of matched beam optics parameters and a multiparticle beam dynamics analysis.

1 Basic Design Choices

Linac4, originally developed as the normal-conducting section of the Superconducting Proton Linac (SPL) [1], is intended to replace the present 50 MeV Linac2. The new linac will inject into the PS Booster (PSB) H^- ions instead of protons at the energy of 160 MeV. This value has been chosen in order to double the $\beta\gamma^2$ factor at PSB injection with respect to the present case. Consequently, the tune shift at PSB injection will be halved, allowing the accumulated beam intensity to be roughly doubled. Linac4 will be installed in the PS South Hall and will re-use part of the LEP RF equipment, e.g. klystrons and waveguides [1].

In the present design, Linac4 is made up of a 3 MeV RFQ, a chopper line, a conventional Drift Tube Linac (DTL) going to 40 MeV, a Cell-Coupled Drift Tube Linac (CCDTL) up to 90 MeV and finally a Side-Coupled Linac (SCL) increasing the beam energy to 160 MeV. While all the other structures operate at 352.2 MHz, the SCL will resonate at twice the basic frequency, 704.4 MHz.

The Side-Coupled Linac structure was developed in the '60s at the Los Alamos National Laboratory for the LAMPF facility [2]. Its peculiarity is that in addition to accelerating cells it also contains coupling cells, placed sidewise (Fig. 1). From the beam point of view, this is a sequence of accelerating gaps operating in the π-mode (180º phase difference between cells), spaced by a distance $\beta\lambda/2$ in order to keep the synchronism between particles and accelerating field. From the RF point of view, it is a bi-periodic chain of resonators (accelerating and coupling cells) operating in the $\pi/2$ mode. In this mode, fields in adjacent cells have 90º phase difference. When the structure is fed into an accelerating cell, all coupling cells have zero fields, while the accelerating cells are excited with the correct polarity. The $\pi/2$ mode is intrinsically stable against perturbations coming from mechanical errors, beam loading etc., meaning that the longitudinal field distribution remains flat even in presence of asymmetries between cells. Stabilisation is obtained because modes around the $\pi/2$ give equal and opposite contributions from perturbations, finally cancelling out [3].

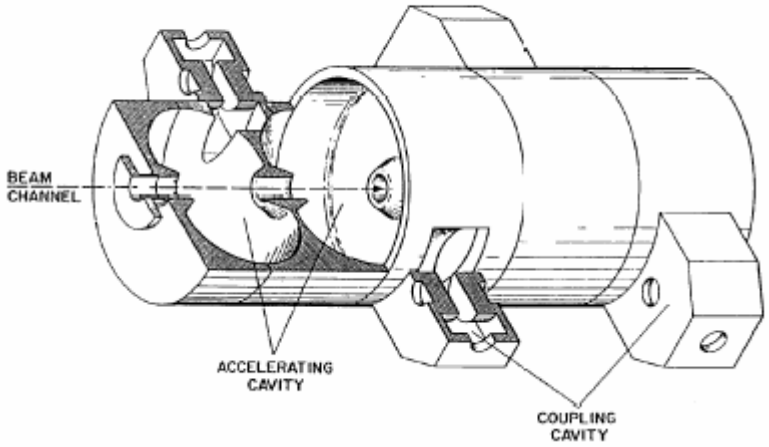

Fig.1. Side-coupled Linac (SCL) schematic.

Tuning of a Side-Coupled Structure corresponds to setting the frequency of the accelerating cells equal to that of the coupling cells, which in turn consists of closing the stop-band in the dispersion curve of the bi-periodic structure (Fig. 2). When the structure is correctly tuned, the accelerating and coupling cell passbands in the dispersion diagram are brought to a confluence. The consequence is that the original operating point of coupled accelerating cells in π-mode (A), with group velocity zero, moves to operating point (B), with non-zero group velocity. When the two passbands are at confluence, all modes contributing to perturbations, i.e. all the modes on the dispersion curve around the operating $\pi/2$ mode, will appear in pairs equally spaced around the $\pi/2$ mode. In presence of a "perturbation" (small asymmetry in the chain of resonators) the new ("perturbed") field will be a linear combination of all modes in the dispersion curve, but modes from the upper and lower branches of the dispersion curve will give equal contributions with opposite sign, finally cancelling out.

The SCL is the ideal accelerating structure for electron and proton beams in the velocity range $0.4 < \beta < 1.0$, providing a higher shunt impedance than DTL or CCDTL, thanks to the doubled RF frequency and to the operation mode, with twice as many gaps per period as the DTL [3]. In the Linac4 design, the SCL covers the energy range from 90 MeV to 160 MeV corresponding to beta from 0.41 to 0.52. The transition energy between CCDTL and SCL corresponds to the point where the shunt impedance of the SCL becomes

higher than that of the CCDTL, which decreases rapidly with the particle beta. The increase in particle velocity in the high energy SCL tanks is much smaller than in a DTL or CCDTL, allowing for the additional simplification of using cells of identical length in a given tank.

The SCL structure is divided into tanks containing a fixed number of cells. Between tanks are placed focusing quadrupoles. More tanks can be connected to form an RF structure fed by a single RF power source, by using a bridge coupler across the quadrupole. The basic SCL layout is represented in Fig. 3.

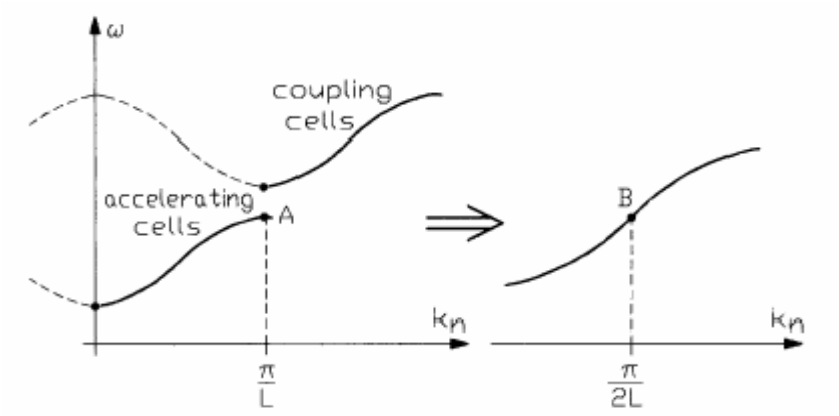

Fig.2. Confluence of two passbands.

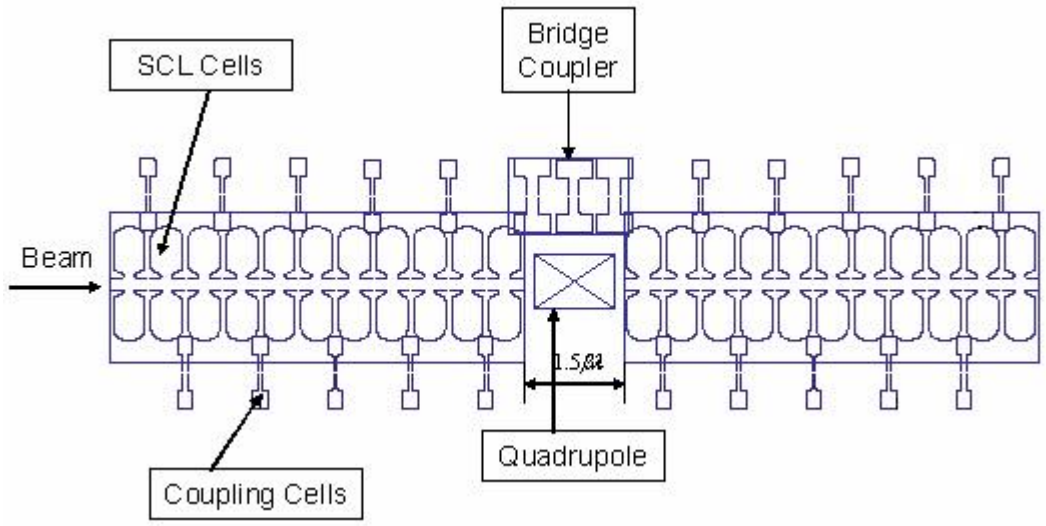

Fig.3. Cross-sectional view of two SCL tanks with bridge coupler.

The starting design choices for the SCL were the following:

- For beam dynamics stability, the same focusing period as the preceding CCDTL is maintained (FODO focusing, 11 cells/tank) [1].
- To minimise the RF costs, the highest possible power is required from the klystron. Preliminary contacts with klystron manufacturers and the experience of the SNS linac at ORNL [4] indicate that a power of 4 MW is achievable by a pulsed klystron at 704 MHz. In the design a maximum power of 3.5 MW per module has been assumed.
- Depending on the klystron power, a module could be made of four or five tanks, each with 11 accelerating cells and ten coupling cells.
- The aperture radius is defined to be 16 mm (i.e. about eight times rms beam size, the standard safety margin taken for Linac4/SPL).

- The coupling slots between accelerating and coupling cells will be re-machined, to control the cell-to-cell coupling factor.
- The tanks will be connected by three-cell Bridge Couplers, as successfully realised on the LIBO medical accelerator [5]. The distance between tanks is fixed at 1.5 βλ, to allow sufficient space for quadrupole, bellows, flanges and some diagnostics.

2 2-D Cell Design

The geometry of the cells for different energies along the SCL was first simulated by SUPERFISH [6]. The goal of these simulations was to compute quality factor, shunt impedance and peak field for different energy values. The shunt impedance is defined as:

$$ZT^2 = \frac{(E_o T)^2}{P / lc}$$

where E_o is the average field on axis, T is the transit-time factor, P is the power loss on the walls and lc is the cavity length. For each cell, shape and gap length are optimised in order to maximise the shunt impedance, keeping constant some dimensions defined by mechanical requirements. The septum thickness (i.e. the distance between the flat parts of adjacent accelerating cells) is fixed at 15 mm, to provide space for cooling channels.

The aperture radius has been fixed at 16 mm. This parameter affects significantly the shunt impedance; however, this relatively large value is required to provide a sufficient margin against halo particles loss when operating at high average currents for the SPL.

An approximate cost analysis indicates that an accelerating gradient $E_o = 4$ MV/m corresponds roughly to the minimum of structure and RF cost and has been assumed as the design gradient for the SCL. At this gradient, the peak surface field is not a critical parameter, and the simulations show that the maximum electric field level is always kept below 1.6 Kilpatrick.

In the final tables, a 20% reduction of the shunt impedances is taken from SUPERFISH, to take into account additional losses coming from surface roughness, imperfections, tuners, coupling slots, etc.

Figure 4 shows the profile of SCL accelerating and coupling cells.

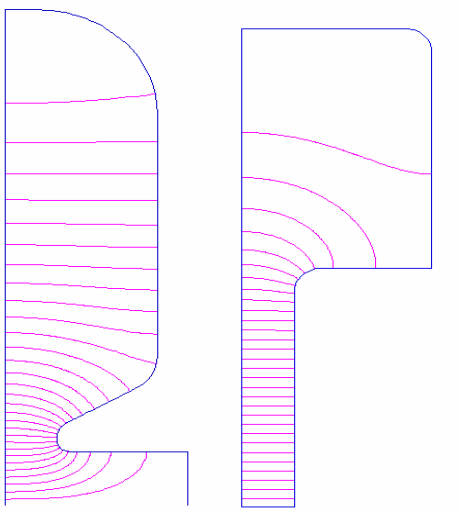

Fig.4. Profile of the SCL accelerating cell for β=0.41 (left) and coupling cell for the first tank (right), with electric field lines.

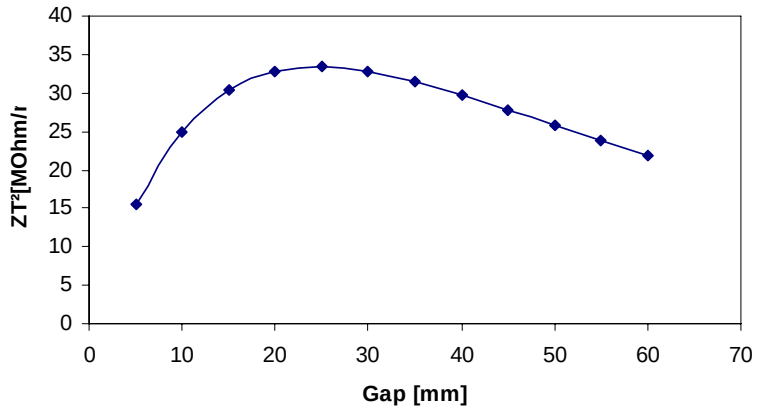

Fig.5. Shunt Impedance vs. gap length for 90 MeV cell.

Figure 5 shows an example of cell optimisation at 90 MeV. For each gap length the shunt impedance is computed, changing the cell diameter to keep the frequency to the design value. For this case, the choice was 25 mm for the gap, corresponding to a shunt impedance of 33.4 MΩ/m.

Table 1 shows the computed SCL cell parameters for different energy values. The computed parameters for coupling and bridge coupler cells are reported in Table 2.

	80 MeV	**100 MeV**	**120 MeV**	**140 MeV**	**160 MeV**	**180 MeV**	**200 MeV**
β	0.388	0.428	0.462	0.492	0.52	0.544	0.566
D (cm)	28.78	28.83	28.99	28.78	28.86	28.81	28.8
L (cm)	8.264	9.108	9.838	10.481	11.06	11.573	12.043
g (cm)	2.1	2.6	3.1	3.4	3.8	4.1	4.4
g/L	0.254	0.285	0.315	0.324	0.343	0.354	0.365
Q	19164.1	20795.1	22120.8	23003	23884.4	24535.9	25119.1
ZT^2 (MΩ/m)	31.532	34.863	37.623	39.771	41.486	42.857	43.98
T	0.89	0.893	0.894	0.897	0.896	0.896	0.895
Ep/E_o	5.996	5.62	5.35	5.374	5.249	5.21	5.17
Ep (Kilp., 3.5MV/m)	0.853	0.799	0.761	0.764	0.746	0.741	0.735
ZT^2 (3% Coupling)	28.928	31.984	34.516	36.487	38.061	39.318	40.349

Table 1: Main accelerating cell parameters (SUPERFISH) for the SCL.

	Coupling Cell	**Bridge Coupler Side Cell**	**Bridge Coupler Mid Cell**
D (cm)	20	20	20
L (cm)	7	12.9	15
Left gap L (cm)		2.529	
Right gap L (cm)		4.29	
g (cm)	1.942	6.081	5.368
g/L	0.277	0.471	0.359
Q	12183.3	14649.4	14937.5
Z (MΩ/m)	67.331	66.844	63.358
Ep (Kilpatrick, 1 MV/m)	1.256	1.613	1.769

Table 2: Main coupling and bridge coupler cell parameters for the SCL.

3 3-D Design

After the 2-D cell design, a 3-D design step is required to determine the coupling factor between accelerating and coupling cells, which is related to the dimensions of the coupling slot (see Fig. 6). The Microwave Studio 3-D RF simulation package was used for these calculations. First of all, the cell geometries found with SUPERFISH were modelled into Microwave Studio. The basic unit is composed by two half accelerating cells and one coupling cell (Fig. 6), with the two half accelerating cells terminated with metallic boundaries. Then, the gaps of the cells are slightly modified, in order to tune approximately the coupling cell to the frequency of the accelerating cell (closed stop band condition). The difference between 2-D and 3-D frequencies is mainly due to the effect of the coupling slot, which is not taken into account in 2-D and reduces the cell frequencies. Finally, the three coupled frequencies of the basic unit are computed and used for the determination of the coupling factor. It must be mentioned that this simple basic unit does not take into account second neighbour couplings, whose relatively small contribution can be neglected at this stage of the study.

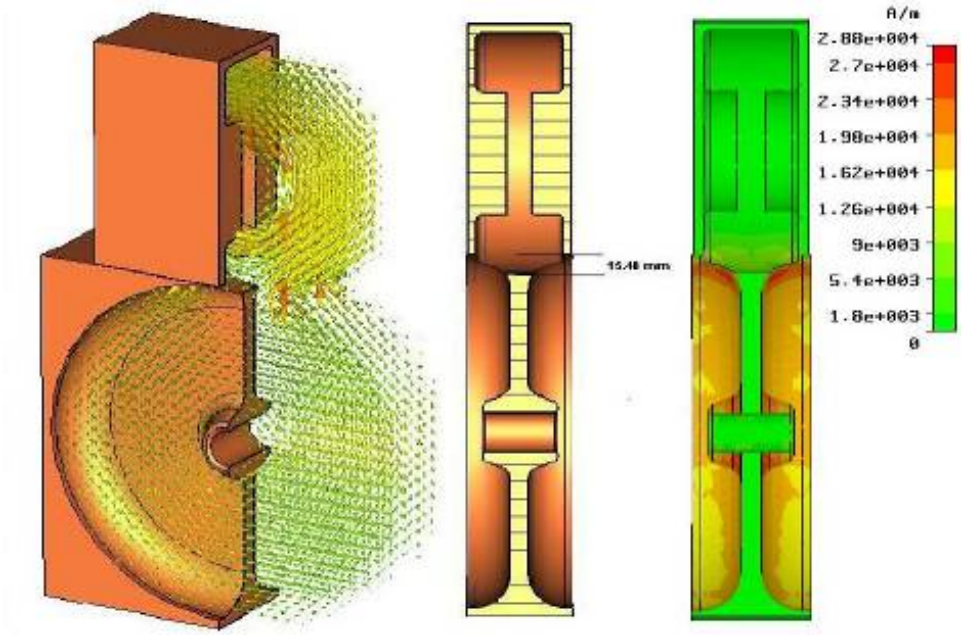

Fig. 6. One coupling and two half accelerating cells as simulated by Microwave Studio. On the left, is shown the magnetic field while the cut-away in the middle indicates the dimension of the coupling slot. The cut-away at right shows the surface current for the accelerating mode.

The dimension of the coupling slots determines the coupling factor but at the same time affects the shunt impedance value. The reduction in ZT^2 is roughly proportional to the coupling, as a consequence of the modified current path in the accelerating cell. The optimum coupling factor is thus a compromise between overall stability of the SCL module, which increases with coupling, and shunt impedance, which instead decreases with the coupling. The preliminary design goal was for a coupling factor of 3%, considered as a satisfactory compromise between the two conflicting requirements.

The coupling factor between cells corresponds to the coupling coefficient in the equivalent circuit model, where the coupled cells are represented as magnetically coupled resonant circuits. The system of three coupled oscillators can be described in terms of three parameters, the accelerating cell frequency f_a , the coupling cell frequency f_c and the coupling factor k. When coupled together, the system of three resonators will oscillate in three modes, with frequencies f_1, f_2, f_3 corresponding to the three modes allowed in this system (0, $\pi/2$ and π), determined by the 3-D simulation. A simple calculation allows the coupling cell frequency to be related to the simulated frequencies:

$$f_c = \frac{1}{\sqrt{1/f_1^2 - 1/f_2^2 + 1/f_3^2}}$$

And finally the coupling factor k can be calculated from the coupling cell frequency and the simulated frequencies:

$$k = \sqrt{1 - \left(\frac{f_c \cdot f_2}{f_1 \cdot f_3}\right)^2}$$

The above technique was used to analyse the influence of slot dimensions on the coupling factor. In the calculations, the distance d between the axis of accelerating and coupling cell was varied. The slot being the intersection between these two volumes, the value of d defines the dimension of the slot and therefore the coupling factor. The coupling calculation is shown on the left side of Fig. 7, whereas the corresponding reduction in Q-value obtained from the simulations is shown on the right side. The 3% coupling factor corresponds to 15 mm distance between the axis of the two cells and leads to a reduction in the Q-value by a few percent.

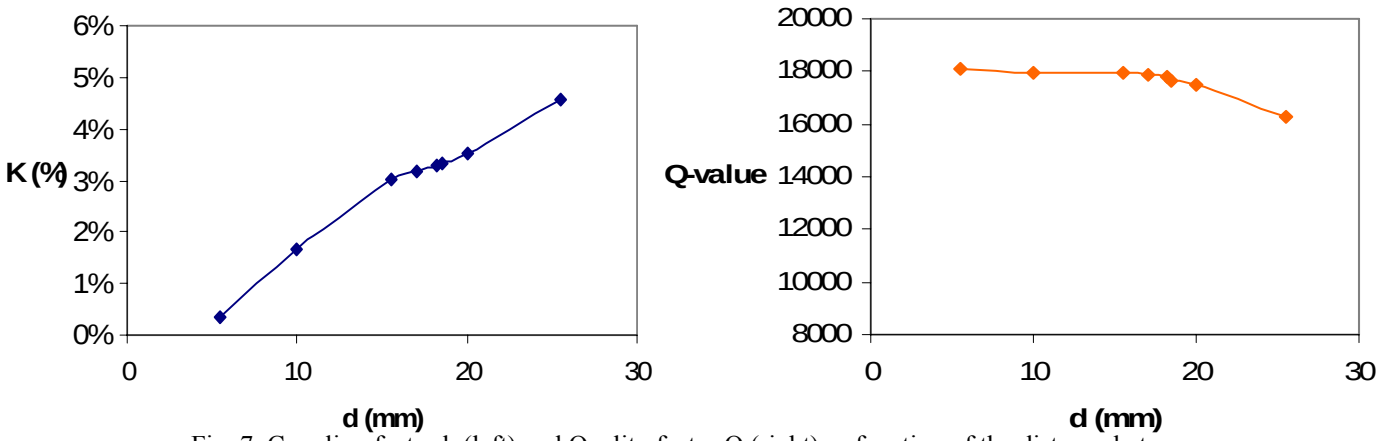

Fig. 7. Coupling factor k (left) and Quality factor Q (right) as function of the distance between accelerating and coupling cell axis.

It is interesting to report that in parallel to these simulations with Microwave Studio, a set of simulations with the 3-D package HFSS were performed at the LPSC laboratory in Grenoble, using the same input geometry [7]. Table 3 shows a comparison of results obtained with the two codes, for a 3% coupling and a cell at 90 MeV. The difference between the two codes comes from the different meshing, in particular in the critical slot region, and gives an idea of the accuracy for this type of calculation.

	d (mm)	f_1 (MHz)	f_2 (MHz)	f_3 (MHz)	f_a (MHz)	f_c (MHz)
µWS	15.48	692.26	702.42	713.47	702.42	702.83
HFSS	20	691.23	701.44	712.62	701.44	701.92

Table 3. Comparison of cell parameters (3% coupling, 90 MeV) computed by Microwave Studio (µWS) and HFSS.

The coupling slot resulting from the intersection of accelerating and coupling cell has a characteristic quasi-elliptical shape, terminating in two sharp edges. Small mechanical errors in the machining and relative positioning of the two cells would lead to appreciable differences in the length of the slot that in turn transform into errors in the coupling coefficient and in the relative cell field. In order to reduce this type of error the slot between accelerating and coupling cells can be re-machined giving a rectangular-like profile. This technique was used in LIBO, and gave excellent results. A set of Microwave Studio simulations was performed to find the correct dimensions for a square slot in the Linac4 SCL. Figure 8 shows the two types of coupling slot.

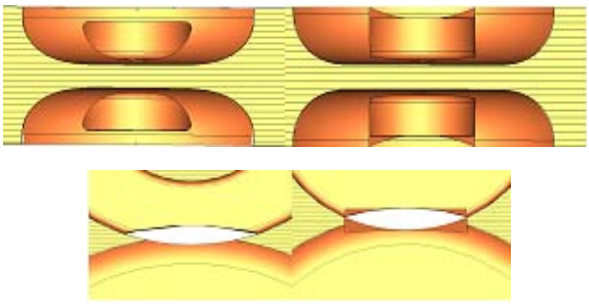

Fig.8. On the left the elliptical slot, on the right the square slot (top view on the top and profile view on the bottom).

The square slot has the same length and width as the common elliptical shape. Figure 9 shows the size of square slot required in order to provide the 3% coupling factor.

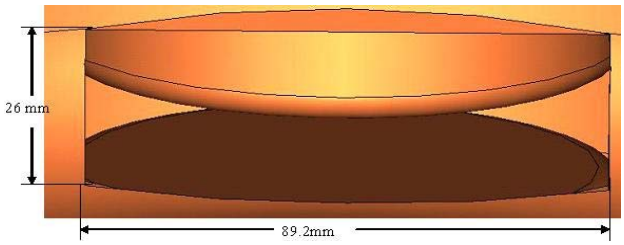

Fig.9. Dimensions of the square slot for 3% coupling.

4 Bridge Coupler Design

The three bridge coupler cells resonantly connect two adjacent tanks. The two side cells of the bridge coupler are coupling cells, while the central cell behaves as an accelerating cell. The latter is excited during operation and can be used to couple the power from the klystron. 3-D simulations of the bridge coupler were performed in order to find the dimensions of the cells and the size of the slots between bridge coupler cells. The coupling factor between bridge coupler cells does not need to be the same as between the cells in the tanks, and there is an economical advantage in going towards high coupling, because this reduces the field level in the central cell of the bridge coupler and therefore the power dissipation there. However, a too low field in the central bridge coupler cell would make the coupling from the waveguide more difficult.

Four different dimensions of the bridge coupler slot (between central and side cells) were analysed with Microwave Studio and are given below. The first one keeps the 3% coupling as in the tanks, while the others allow for increasing the coupling between bridge coupler cells.

- Bridge coupler coupling is the same as tank coupling, namely 3%
- Bridge coupler coupling the tank 7%
- Bridge coupler coupling the tank 11%
- Bridge coupler coupling the tank 15%

For every case, four different bridge coupler slots were simulated (Fig. 10), in order to compare the losses in the central bridge coupler cell for different slot geometries. Finally, the first coupling geometry was adopted, for a 3% coupling, as in the tanks.

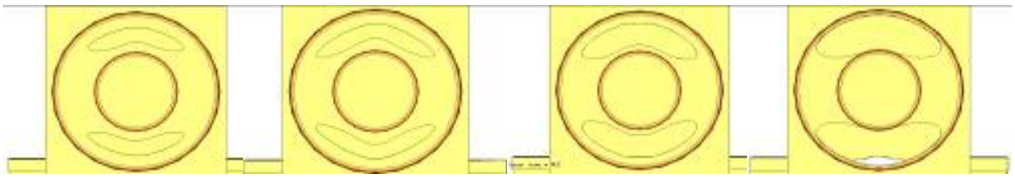

Fig.10. Four different slots between the side and mid bridge coupler cells.

The resulting geometry for the transition between tank and bridge coupler is shown in Fig. 11.

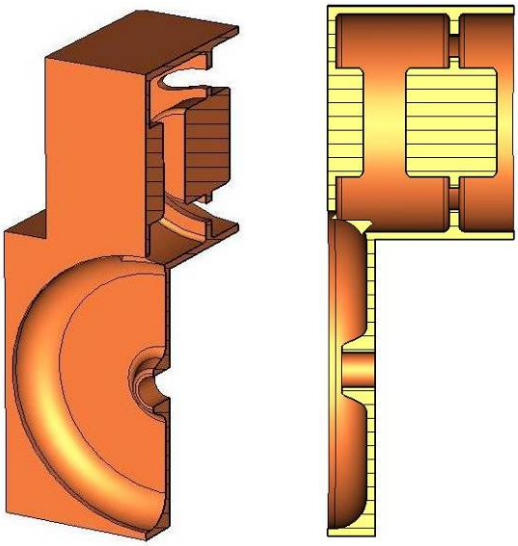

Fig.11. Perspective and front view of last half accelerating cell of the tank and bridge coupler coupling cell and half central cell.

5 Error sensitivity of SCL Modules

A calculation of the stability (sensitivity to cell frequency errors) of a long SCL module is required to support the choice of 3% coupling. The technique adopted for this calculation consists of representing a tank with its equivalent circuit, made of 21 coupled oscillating circuits (11 for the accelerating cells and ten for the coupling cells) (Fig. 12). A frequency-domain analysis of this circuit with the PSPICE circuit emulator gives the frequencies of its 21 resonance modes, and for each mode provides the field level (voltage) in each oscillating circuit. For the operating $\pi/2$ mode, the voltage is the same in all the resonating circuits representing accelerating cells, and zero in those representing coupling cells.

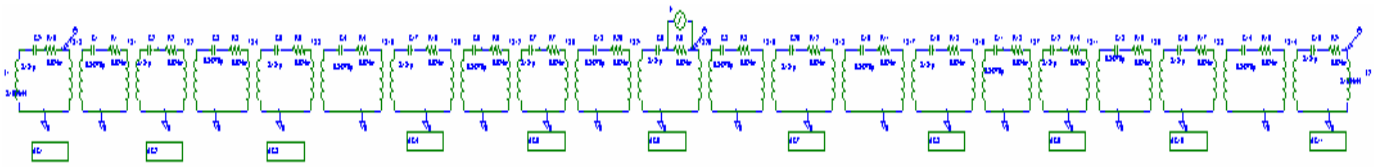

Fig. 12.: Circuit model for the first SCL 11-cell tank.

Subsequently, in this model errors coming from machining tolerances and from the limitations in the cell tuning can be introduced in the form of frequency errors on the individual oscillating circuits. The effect of

these errors will be a deviation from the nominal flat voltage distribution in the accelerating cells, in the form of additional mode components superimposed on to the nominal flat distribution. The overall field error can be computed, and compared to the original cell error distribution. The calculation can be limited to one tank in order to reduce the size of the circuit and the simulation time. The field error is proportional to the number of cells in the chain and the error for a five-tank module will be five times the error for one tank.

In order to represent a situation close to a real case, two types of error were introduced:

1. a small difference in frequency between the coupling cells and the accelerating cells, representing the remaining "stop band" at the end of the tuning process. A stop band of 200 kHz was assumed for the calculations, based upon an estimation of the accuracy in coupling cell tuning and on the experience with the LIBO SCL.
2. a statistical spread in the frequencies of the accelerating cells, remaining after the tuning of each accelerating cell by deformation ("dinging"), estimated at ±50 KHz.

A statistical analysis with 60 uniform random error distributions in the accelerating cells with amplitude ±50 KHz was performed for different values of the coupling factor k. Then another set of 60 cases was computed, with errors in both accelerating and coupling cells. For each calculation the resulting maximum field error, i.e. the maximum of ΔV/V between cells, was reported. The results are shown in Fig. 13.

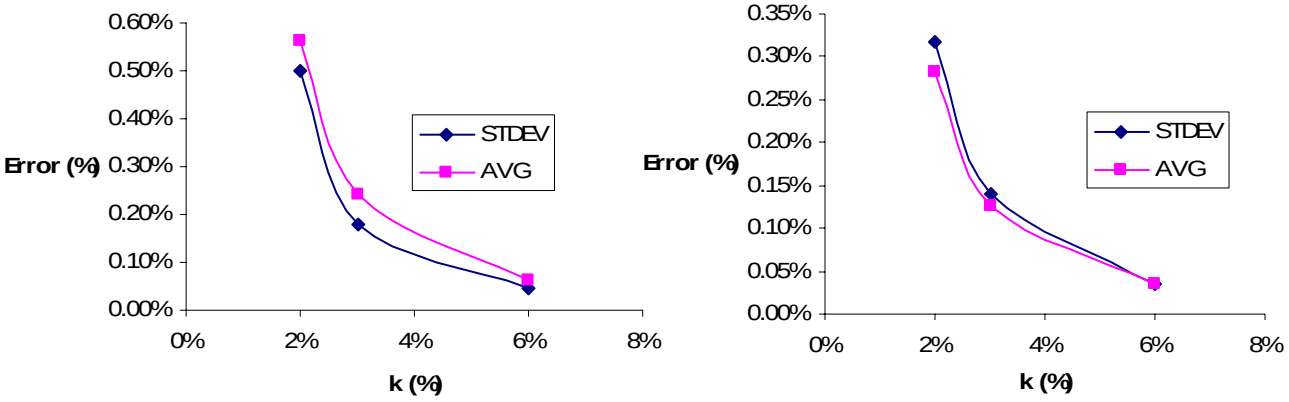

Fig.13.: Average field error in a tank and standard deviation (60 random error distributions) for ±50 KHz random errors in the accelerating cells (left) and in accelerating and coupling cells (right). In both cases a stop band of 200 KHz is assumed.

From the above curves can be estimated the overall field error in an SCL module with 3% coupling. Conservatively taking a maximum error equal to the average plus two standard deviations (i.e. 98% of real cases will be within this limit) we calculate from the left curve of Fig. 13 a maximum error of about 0.6% for a 3% coupling. Multiplying this figure. by 5, to take into account the fact that a module is composed of five tanks, a total error of 3%, i.e. ±1.5% from the mean field value is obtained. This error is still well below the usual tolerance on field adjustment (±2.5%) and within the beam dynamics tolerances. However, from Fig. 13 it can be seen that a further reduction of the coupling factor would immediately increase the field error, while the gain in Q-value (Fig. 7) would be minimum. As a result of this analysis, the coupling factor of 3% is confirmed as an optimum choice for the SCL.

It is interesting to observe that the error varies as $1/k^2$. This dependence can be explained by coupled oscillator theory [8]. Moreover, comparing the two curves in Fig. 13 one can see that errors in the frequencies of the coupling cells tend to compensate the effect of errors in the accelerating cells, and that the field error is lower in presence of a spread in both accelerating and coupling cell frequencies.

6 SCL Layout Design

In order to define the overall SCL layout and to perform a preliminary beam dynamics analysis two codes developed at LANL, DESIGN and LINAC were used [9]. DESIGN starts from the cell parameters calculated

with SUPERFISH, including a correction for the slot effect. First of all, the code defines the optimum beta for each tank as the one minimising phase slippage, i.e. the deviation in synchronous phase coming from the fact that all cells in a tank are identical. Then it calculates energy gain and power consumption for each tank and adds up the number of? tanks to build a complete structure, using accelerating gradient, number of cells per tank and intertank distance provided by the user.

The parameters for the layout calculated by DESIGN are given in Table 4. Twenty tanks are needed to cover the range from 90 MeV to 160 MeV, for a design gradient of 4 MV/m.

Operating Frequency [MHz]	704.4
Input Energy [MeV]	90
Output Energy [MeV]	161.2
Aperture Radius [mm]	16
Number of Cells/Tank	11
Number of Tanks/Module	5
Number of Modules	4
Total Number of Tanks	20
Number of Klystrons	4
Number of Quadrupoles	20
Quadrupole Gradient [T/m]	17.1
Total Length [m]	27.78
Tank Length [mm]	$964 \rightarrow 1214$
Tank Diameter [mm]	$283 \rightarrow 290$
Quadrupole Length [mm]	100
ZT^2 [MΩ/m]	$23.8 \rightarrow 29.1$
Peak Electric Field (Kilp. units)	0.86
Gradient E_o [MV/m]	4
Synchronous Phase Angle [degree]	-25
Total RF Power [MW]	14.2

Table 4. Main layout parameters of SCL.

7 Beam Dynamics

The quadrupoles in the SCL will be arranged in a conventional FODO lattice, with quadrupoles placed between tanks. The matched Twiss parameters and the quadrupole gradients have been calculated with the envelope code TRACE3D [10], while multiparticle beam dynamics simulations have been performed with the LINAC code [9]. LINAC is a version of the code PARMILA from the Los Alamos Laboratories, adapted for SCL structures. It reads the output data of DESIGN. A 6-D waterbag distribution space-charge was used as input distribution, with a beam current of 60 mA distributed into $5 \cdot 10^4$ macroparticles. The value of the current takes into account the fact that bunch current is doubled by the frequency jump between 352 and 704 MHz. Input emittances (normalized) are 0.275, 0.281 and 0.373 π mm mrad.

The tune ratios for all SPL/Linac4 ? have been selected in order to operate the machine in a stable area of the Hofmann chart [11], given in Fig. 14.

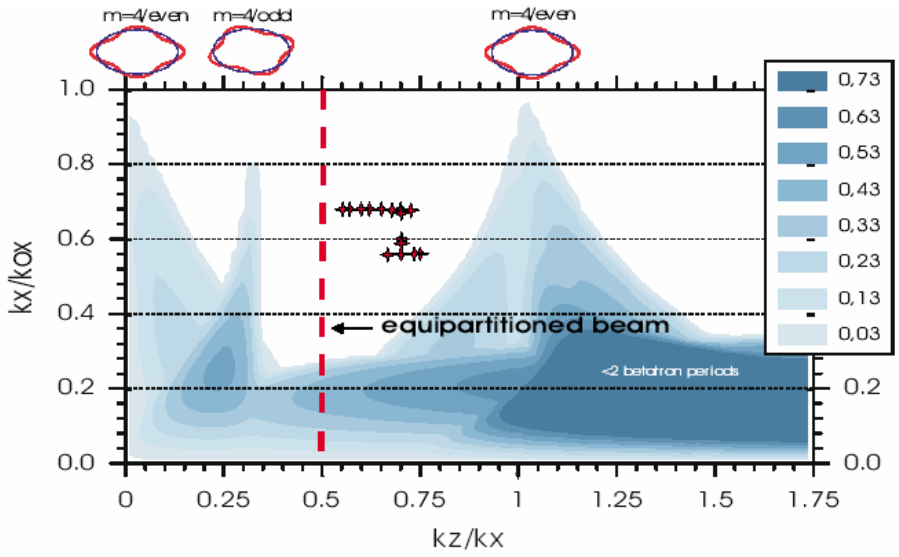

Fig.14. Hoffman's stability chart for an emittance ratio of 2. Graduations indicate the growth rates of resonances in terms of transverse betatron periods. Stability is expected in white regions.

A tune ratio $\sigma_l / \sigma_t \sim 0.7$ (k_z/k_x in Fig. 14) was retained for the beam dynamics design of all Linac4-SPL ?, in order to obtain a strong transverse focusing and a smaller transverse beam size while operating in a stable region close to equipartitioning. While the longitudinal phase advance is defined by the choice of accelerating gradient and synchronous phase (-25°), the transverse phase advance can be adjusted by the choice of quadrupole gradients in order to obtain the required tune ratio. Different simulations were made keeping the same longitudinal settings but different quadrupole adjustments. In the final optics, the maximum transverse zero current phase advance is σ_t=124.6° per period and the maximum longitudinal zero current phase advance is σ_l=85.3° period. The ratio σ_l / σ_t is about 0.68. The corresponding gradient for the quadrupoles, which have a length of 100 mm, is 17.1 T/m. Figure 15 shows the matched beam and phase advance for first SCL period, as computed by TRACE3D.

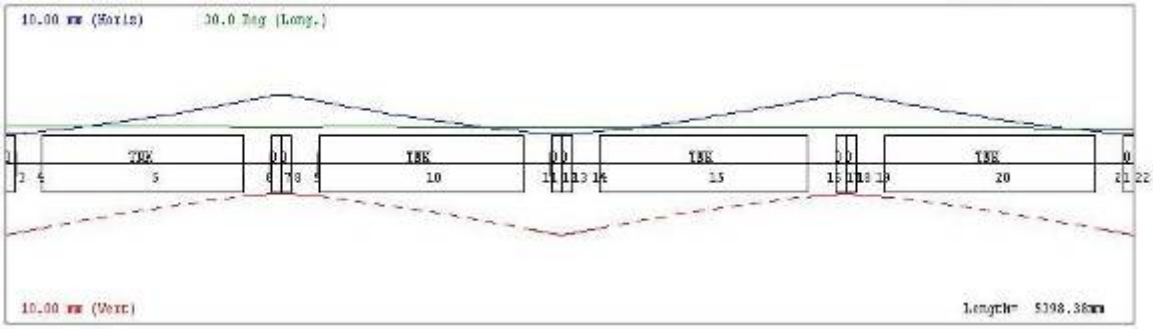

Fig.15. Beam envelopes in the first period, as computed by TRACE3D. Horizontal vertical and longitudinal envelopes are shown.

After the envelope calculations, the program LINAC was used for a multiparticle calculation and a preliminary estimation of the emittance growth, computed in 0.3 % transversally and 1.66 % longitudinally. Figure 16 shows the behaviour of emittances along the SCL structure.

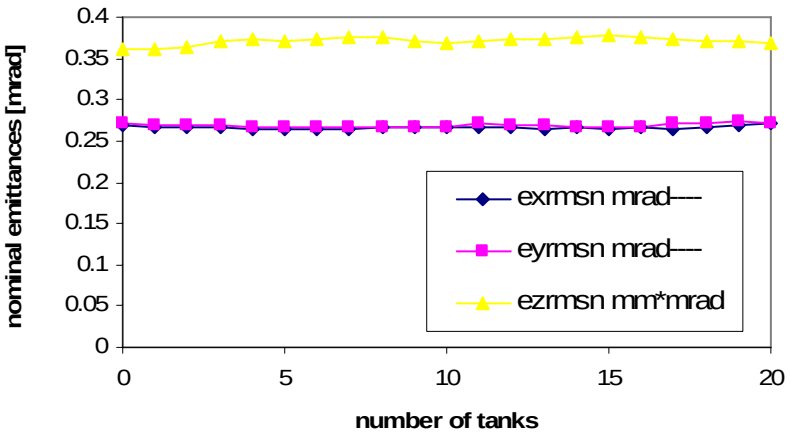

Fig.16. The nominal emittance behaviour along the twenty SCL tanks.

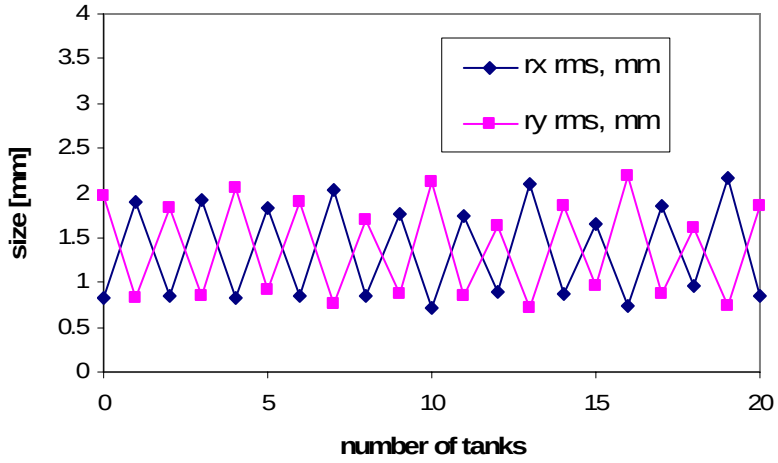

Fig.17. Transverse beam size along the SCL structure (centre of quadrupole).

Figure 17 shows the rms beam radius in x and y in the centre of the quadrupoles along the SCL. The matching is satisfactory and maximum rms radius is about 2.1 mm, giving a comfortable safety factor of 7.5 between aperture and maximum rms beam size.

Figure 18 shows the evolution of rms energy spread along the SCL.

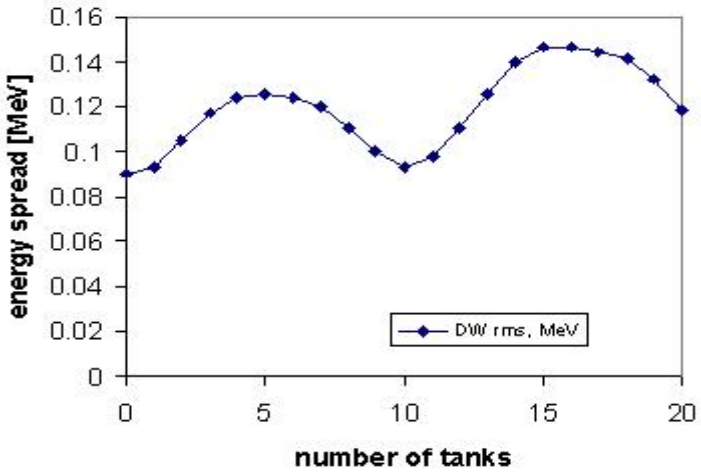

Fig. 18. Nominal energy spread along the twenty SCL tanks.

Figure 19 shows the phase space diagrams computed by LINAC.

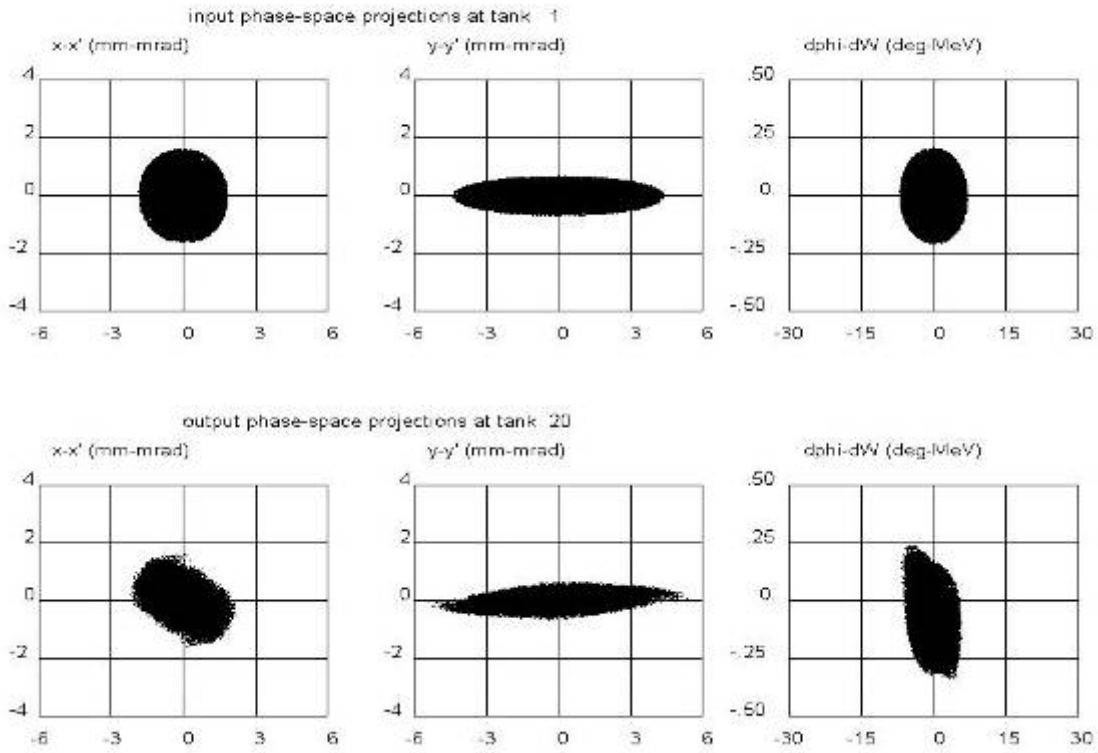

Fig. 19. Input nominal beam emittances in the SCL (top graphs) and output emittances as computed by LINAC (bottom graphs).

It is interesting to compare the output SCL emittances computed by LINAC with those obtained by F. Gerigk with the code IMPACT, using the same input parameters [12]. IMPACT is a modern code that takes into account field maps for the RF gaps (while LINAC approximates a gap with a thin lens) and uses up to several millions macroparticles for halo calculations. Transverse and longitudinal emittances obtained with IMPACT at the end of the SCL are shown in Fig. 20. The agreement with the LINAC results is good, and justifies the use of a simpler code for this level of SCL design.

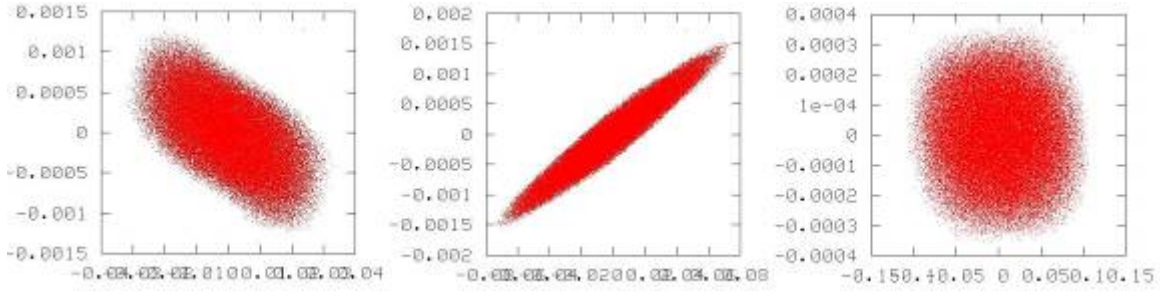

Fig.20. Emittances for the nominal case simulated by Impact along the normal conducting part of the SPL.

Another beam dynamics code that was tested on the SCL was DYNAC, a relatively new code partly developed at CERN [13]. This code makes use of on-axis field maps calculated by SUPERFISH, turning them into the form of a Fourier series expansion. Two cases were studied, with $5 \cdot 10^4$ particles, using two different space charge routines, SCHEFF and HERSC. HERSC is a 3-D routine that provides the analytical solution of the electrostatic Dirichlet-Neumann problem within an arbitrary bunch and is ideal for highlighting halo formation. SCHEFF is a 2-D (r-z) routine that considers rings of elementary charge.

Emittance growth for DYNAC is higher than for LINAC. The transverse emittance growth is 1.4% using SCHEFF and 2.4% using HERSC. The corresponding longitudinal emittance growth was 9.4% and 7.4%

respectively. Figure 21 shows the energy spread and the phase advance along the SCL, Figure 22 shows the output emittances and the corresponding transverse envelopes are shown in Fig. 23.

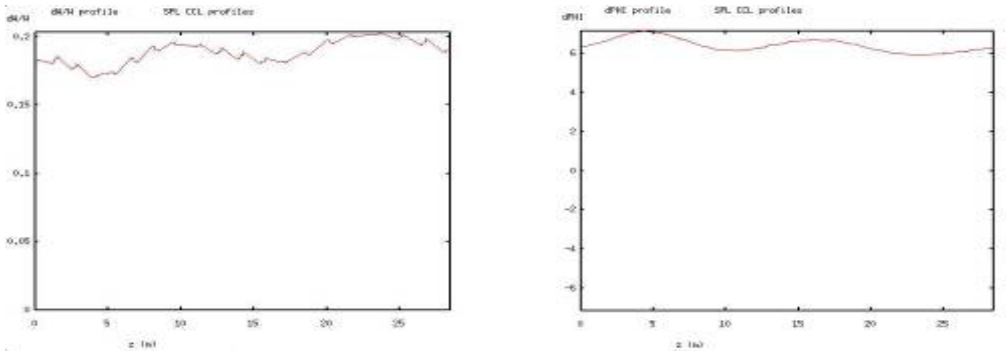

Fig. 21. Energy spread (right) and phase advance (left) along the SCL, as computed by

.

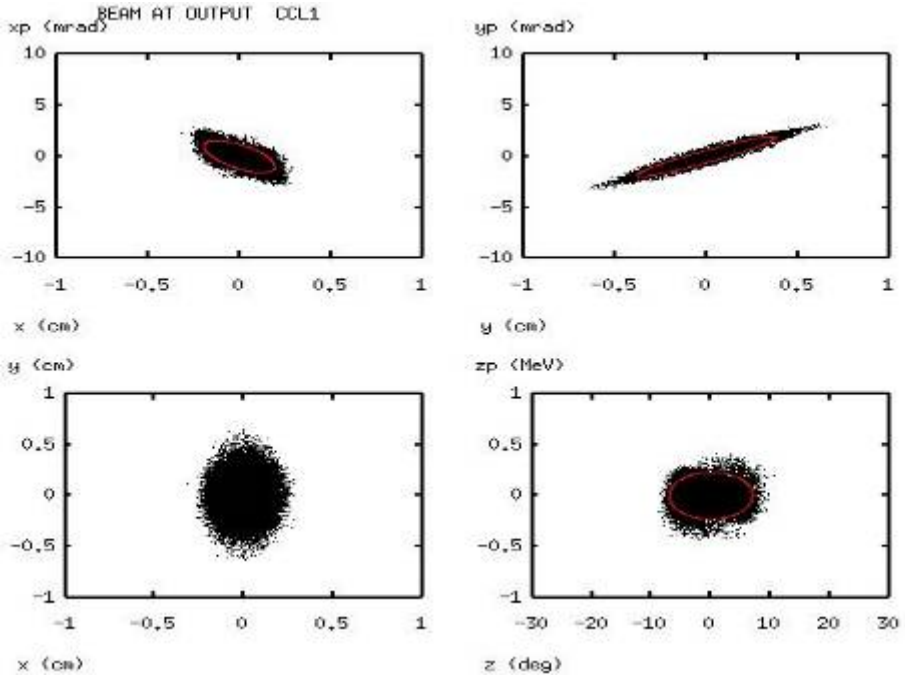

Fig. 22. Output emittances computed by DYNAC using SCHEFF space charge routine.

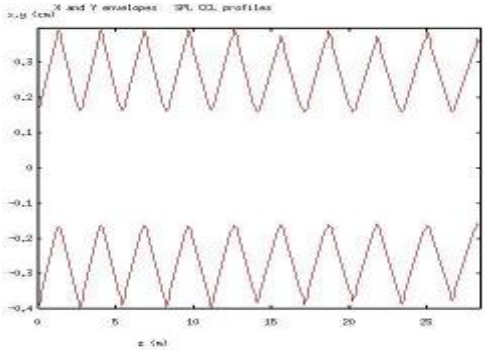

Fig. 23. X and Y envelopes computed by DYNAC.

Figure 24 shows a comparison of transverse and longitudinal emittance growth for three cases, the differences coming from the different space charge routines. It must be mentioned that when analysing this design with other codes like IMPACT or PATH the results are in better agreement with LINAC than with DYNAC [14].

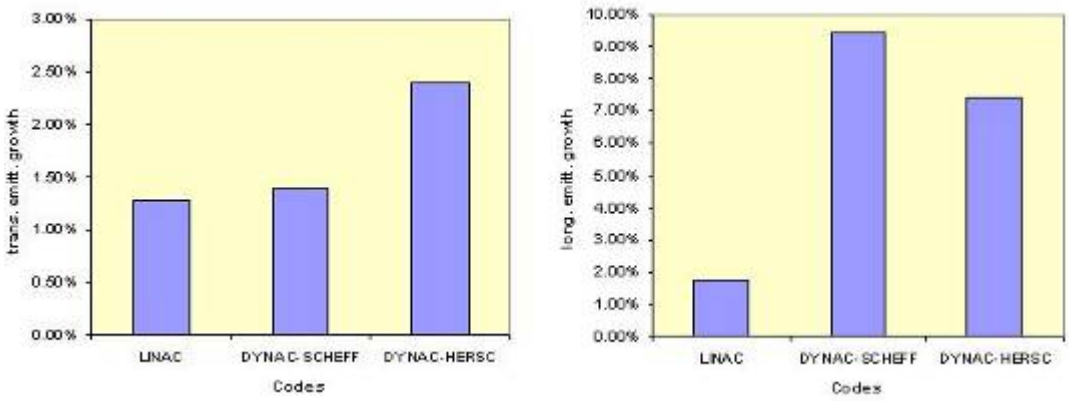

Fig.24. Comparison of transevsal and longitudinal emittance growth for each case.

8 Comparison of Alternative Tank Layouts

The number of cells per tank is an important parameter for the design of the SCL. A large number of cells leads to longer focusing periods and to a larger beam size, while a small number of cells reduces the actual accelerating length of the SCL and requires more bridge couplers, decreasing real estate gradient and RF power efficiency. In the preliminary design, the number of cells per tank has been fixed at 11. This figure needs to be optimised once the beam dynamics design procedure has been set up.

Three different numbers of cells per tank (namely 9, 11 and 13) have been considered, and the sequence of codes DESIGN, TRACE3D and LINAC has been applied for each of the three cases. The gradient is fixed to 4 MV/m for all cases. The current is set to 60 mA and the number of particles used is $5 \cdot 10^4$.

In the case of nine cells per tank, the number of tanks is increased to 25, while for 11 and 13 cells the number of tanks is 20 and 17 respectively. The total length of the SCL is 29.8, 27.8 and 27 m for 9, 11 and 13 cells/tank respectively. For all cases the phase advance has been determined in order to keep a ratio of 0.7 between longitudinal and transverse phase advance. Figure 25 shows the transverse phase advance per metre at the centre of the SCL for the three cases.

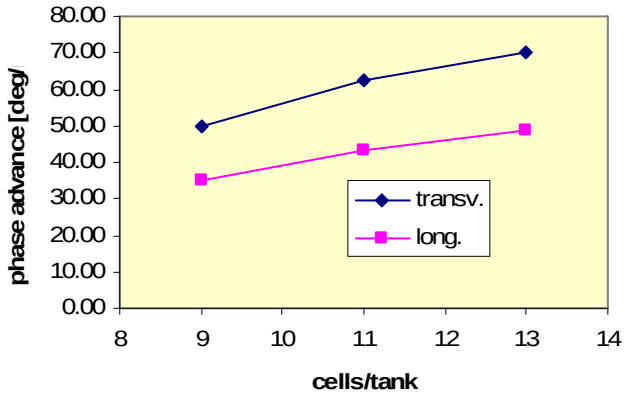

Fig.25. Comparison of the phase advance for 9, 11 and 13 cells per tank.

Figure 26 shows the values of emittance growth, indicating that there is a tendency to larger transverse emittance growth with longer focusing periods. The main difference between the three cases is in the envelopes (Fig. 27) and in beam size (Fig. 28, taken again at the centre of each quadrupole).

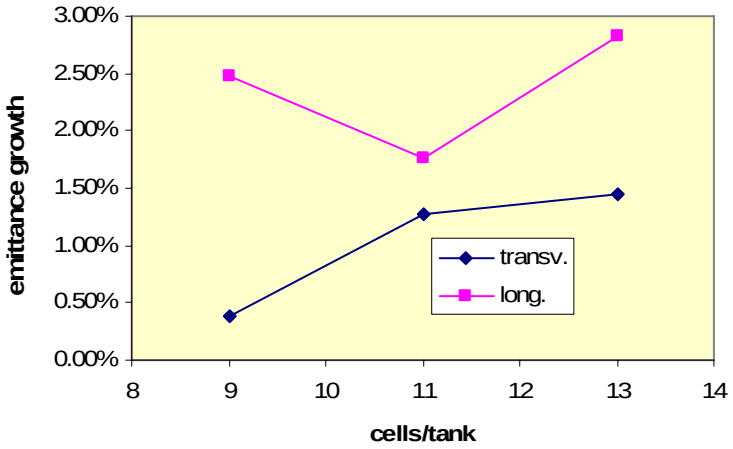

Fig.26. Comparison graph of the emittance growth.

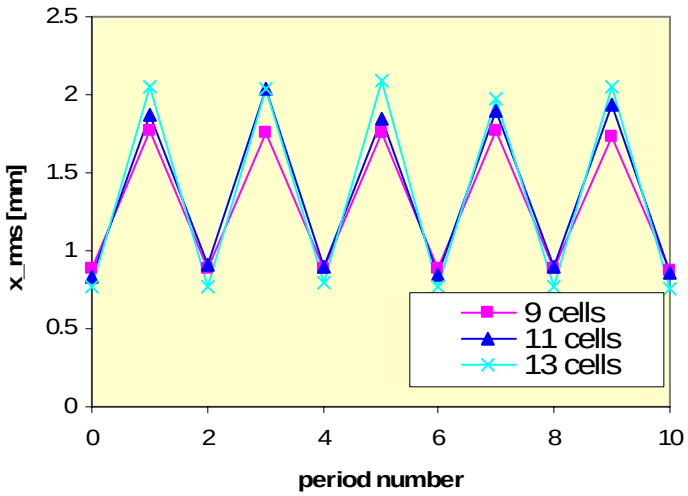

Fig.27. Comparison of envelopes X and Y.

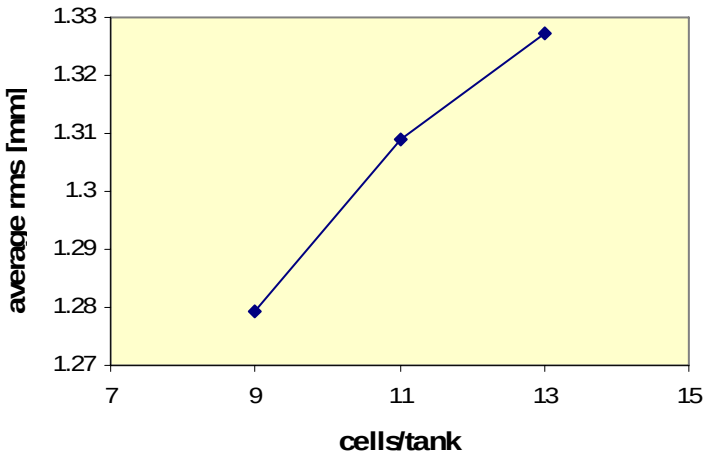

Fig.28. Beam size for three cases.

The conclusion of this analysis is that there is only a small difference in beam properties between the three test cases, the most evident one being as expected the beam size. However, no particular reasons appear in favour of moving away from the nominal 11 cells/tank design.

9 Acknowledgments

The authors wish to thank F. Gerigk for providing input beam parameters and the IMPACT results, Y. Martinez for the study of coupling and bridge coupler with HFSS, and J.M. De Conto and V.G. Vaccaro for many useful discussions. E. Tanke has kindly provided support for DYNAC.

We acknowledge the support of the European Community-Research Infrastructure Activity under the FP6 "Structuring the European Research Area" programme (CARE, contract number RII3-CT-2003-506395)

10 References

[1] F. Gerigk, M. Vretenar, Design Choices for the SPL Normal-Conducting Front End (3-120 MeV). CERN-NUFACT-NOTE NF 110, CERN, Geneva, 2002.
[2] E.A. Knapp, B.C. Knapp and J.M. Potter, Standing Wave High Energy Linear Accelerator Structures, Review of Scientific Instruments, Volume 39, Number 7, pp. 979-991.
[3] T.P. Wangler. Principles of RF Linear Accelerators. Ed. Wiley Series in Beam Physics and Accelerator Technology. Los Alamos National Laboratory, Los Alamos, New Mexico, 1998.
[4] N. Bultman,; J. Billen, Z. Chen, M. Collier, D. Richards, L. Young, Fabrication and tuning of the SNS CCL hot model. PAC 2003- pages 2844, Portland, USA, 12 - 16 May 2003.
[5] P. Berra, S. Mathot, E. Rosso, B. Szeless, M. Vretenar, U. Amaldi, K. Crandall, D. Toet, M. Weiss, R. Zennaro, C. Cicardi, D. Giove, C. De Martinis, D. Davino, M.R. Masullo, V.G. Vaccaro, Study, Construction and Test of a 3 GHz Proton Linac-Booster (LIBO) for Cancer Therapy. Proceedings of EPAC 2000, pp. 2495-2497. Vienna, Austria, 2000.
[6] J.H. Billen and L.M. Young, *Poisson Superfish*, LA-UR-96-1834.
[7] R. Garoby, Activity Report for the first quarter of 2004. HIPPI Activity Reports. Geneva, JRA3, 30 April 2004.
[8] J.M. De Conto and V. Vaccaro, private communications.
[9] K.R. Crandall, Design and Linac Applications. Private Documentation by K.R. Crandall.
[10] K.R. Crandall, D.P. Rusthoi, TRACE-3D Documentation. Third Edition May 1997. LA-UR-97-886.
[11] F. Gerigk, I. Hofmann, Beam Dynamics of Non-Equipartitioned Beams in the Case of the SPL Project at CERN. CERN-PS-2001-051-RF, CERN-NEUTRINO-FACTORY-NOTE-85, CERN-NUFACT-NOTE-85. Geneva, CERN, 18 July 2001.
[12] F. Gerigk, E. Benedico Mora, A. Lombardi, E. Sargsyan, M. Vretenar, Beam Dynamics for a new 160 MeV H^- Linac at CERN (LINAC4). Linac 2004 Conference. Lübeck, Germany, 2004.
[13] P. Lapostolle, S. Valero, E. Tanke, M. Doleans. Program DYNAC, version 5.5, CERN/PS and CEN/SACLAY, January, 27, 2004.
[14] F. Gerigk, A. Lombardi, private communications.

Annex: Design details

Table 5. Lattice data for the SCL structure.

Tank	Tank Length [mm]	Mid Tank Energy [MeV]	E_0T [MV/m]	ZT^2 [MΩ/m]	Phid [deg]	Total Power [MW]
1	964.42	93.13	3.566	23.8	-26.9	0.69
2	978.69	96.31	3.568	24.1	-26.9	1.38
3	992.83	99.54	3.57	24.4	-26.8	2.07
4	1006.85	102.81	3.571	24.8	-26.8	2.76
5	1020.74	106.13	3.573	25.1	-26.7	3.46
6	1034.5	109.5	3.574	25.4	-26.7	4.16
7	1048.14	112.91	3.576	25.7	-26.6	4.86
8	1061.64	116.36	3.577	26	-26.6	5.57
9	1075.02	119.86	3.579	26.2	-26.6	6.28
10	1088.28	123.41	3.58	26.5	-26.5	6.99
11	1101.4	127	3.581	26.8	-26.5	7.7
12	1114.39	130.63	3.582	27.1	-26.5	8.42
13	1127.26	134.3	3.583	27.3	-26.4	9.14
14	1139.99	138.02	3.584	27.6	-26.4	9.86
15	1152.6	141.78	3.585	27.9	-26.4	10.58
16	1165.08	145.58	3.585	28.1	-26.3	11.31
17	1177.43	149.42	3.586	28.4	-26.3	12.04
18	1189.65	153.3	3.587	28.6	-26.3	12.77
19	1201.74	157.22	3.587	28.9	-26.2	13.5
20	1213.7	161.18	3.587	29.1	-26.2	14.24

Table 6. Simulation results by LINAC and DYNAC.

	LINAC		DYNAC (SCHEFF)		DYNAC (HERSC)	
	in	out	in	out	in	out
$\varepsilon_{x,\ r.m.s,\ norm}$ [mm*mrad]	0.27	0.272	0.271	0.279	0.271	0.283
$\varepsilon_{y,\ r.m.s,\ norm}$ [mm*mrad]	0.271	0.271	0.277	0.277	0.278	0.279
$\varepsilon_{z,\ r.m.s,\ norm}$ [mm*mrad]	0.361	0.367	0.372	0.407	0.372	0.4
$r_{xr.m.s}$ [mm]	0.836	0.847	0.831	0.666	0.831	0.705
$r_{yr.m.s}$ [mm]	1.976	1.861	1.995	1.691	1.995	1.768
$\Delta E_{r.m.s.}$ [MeV]	0.09	0.118	0.187	0.205	0.187	0.213

Table 7. Comparison of 9, 11 and 13 cells/tank.

	9 cells/tank		11 cells/tank		13 cells/tank	
	in	out	in	out	in	out
$\varepsilon_{x,\ r.m.s,\ norm}$ [mm*mrad]	0.271	0.273	0.27	0.272	0.27	0.275
$\varepsilon_{y,\ r.m.s,\ norm}$ [mm*mrad]	0.277	0.277	0.271	0.271	0.279	0.279
$\varepsilon_{z,\ r.m.s,\ norm}$ [mm*mrad]	0.375	0.384	0.361	0.367	0.376	0.384
$r_{xr.m.s}$ [mm]	0.886	1.679	0.836	0.847	0.774	1.994
$r_{yr.m.s}$ [mm]	1.778	0.877	1.976	1.861	2.08	0.777
$\Delta E_{r.m.s.}$ [MeV]	0.098	0.118	0.09	0.118	0.097	0.148
Tanks	25		20		15	
Length [mm]	2984		2778		2686	
Total Power [MW]	14.817		14.24		14.86	